Quantum Chemical Modelling of Hemicellulose Fast Pyrolysis: β-D-xylopyranose as a Structural Motif

J. Lupi[1], M. Kelly[1], A. O'Shea[1], M. R. Ghaani[2], and S. Dooley*[1]

[1]School of Physics, Trinity College Dublin, Dublin, Ireland
[2]School of Engineering, Department of Civil, Structural & Environmental Engineering, Trinity College Dublin, Dublin, Ireland

Abstract

The aim of this research is to investigate the pyrolytic reactivity of hemicellulose, specifically focusing on β-D-xylopyranose (xylose), as it is a significant component of hemicellulose. Quantum chemistry-based computational techniques, such as density functional theory, post Hartree-Fock methods, and composite schemes, were employed to evaluate the potential energy surfaces for the initial steps of xylose thermal degradation pathways. Conformational analysis of minima and transition states was carried out in order to obtain molecular structure guesses for global minima. To compare the accuracy of this study against other approaches, reference data was obtained from "cheap" composite schemes. In addition, the Arrhenius parameters were derived by fitting rate coefficients computed using transition state theory. These findings are beneficial and will be utilized in developing a kinetic model scheme in the near future.

Introduction

Biomass pyrolysis refers to the thermal decomposition of organic matter, such as agricultural waste and wood, in the absence of oxygen to produce biofuels, such as bio-oil, charcoal, and biogas. As the demand for energy grows, biomass pyrolysis has emerged as a promising source of clean and sustainable energy. This is because it produces useful biofuels, and has the potential to reduce greenhouse gas emissions by replacing fossil fuels, while also minimizing waste. For example, the European Union has set targets to increase the use of renewable energy and reduce greenhouse gas emissions [1]. This has led to increased investment in biomass pyrolysis technologies, as well as the development of policies and incentives to support their deployment.

Lignocellulosic plant matter in particular is a highly desirable form of biomass with numerous advantages. Its abundance, widespread availability, and cost-effectiveness make it an attractive option for various applications, owing to its prevalence in crop residues, woody plants, and grasses. Chemicals, fuels, and energy must be produced from lignocellulosic plant matter in order to decarbonize our global economies and, to be successful, these lignocellulose-derived products must compete in quality and price with fossil-derived products. Lignocellulose is formed by three main components, namely cellulose, hemicellulose, and lignin.

Existing models to describe the chemical reaction of lignocellulosic biomass are approximate in detail and empirical in nature [2–8]. For pyrolysis and combustion, most attention has focussed on cellulose, and these models have propagated as archetype to lignocellulose, hemicellulose and lignins. The historical approach has been to arbitrarily partition "gears" of reactivity across structural attributes imposed to the kinetic model architecture.

In order to accurately simulate the chemical reaction of lignocellulose, it is necessary to have a model of its composition. This involves two main challenges: (i) identifying the precise chemical structure of the lignocellulose, and (ii) creating a compositional model that can approximate this structure. Today, useful progress has been made on (i) but compositional models (ii) are basic and limiting to progress [7, 8]. For both the chemical reaction and compositional modelling challenges, the works of Ranzi and co-workers [3–6] have made pioneering progress. Normally, only the elemental composition (C/H/O) of lignocellulose is typically reported [2, 5]. Ranzi and coworkers innovate by inferring the biochemical composition of individual lignins and lignocelluloses by relating their C/H/O elemental composition to that of a set of seven reference species. The approach established by Ranzi et al. is to define pseudo-components (real or virtual model compounds) that contain the main chemical compositional features of actual biomass materials. These pseudo-components are combined in the fractions needed to replicate the C/H/O of the target lignocellulose. The approach is similar to compositional modelling work on liquid fuels by Dooley *et al.* [9]. In both, there are two key aspects; (i) accurate provision of (lignocellulose) chemical functionalities by pseudo-component definition, and (ii) selection and determination of meaningful indicators of lignocellulose composition. The state-of-art practice has been to directly couple this compositional model to the chemical equations and rate constants that constitute the reaction kinetic model. Models of this type are refered as to (lumped) compositional-kinetic models.

For hemicelluloses, Dussan *et al.* [7] and Ranzi *et al.* [6] have both recently implemented and advanced models of the B-S type compositional-kinetic model architecture. In Dussan *et al.*, two "active hemicelluloses"

*Corresponding author: stephen.dooley@tcd.ie

are used to test the applicability of expanded detail to describe wider ranges of reactivity and evolved species fractions as determined by various experimental methods. Concurrently, Ranzi *et al.* also re-parameterized their lumped compositional-kinetic model.

To enhance the present comprehension of lignocellulose pyrolysis, it is necessary to incorporate physicochemical information into kinetic models, which can be acquired through the use of computational chemistry techniques. Particularly, quantum chemistry modelling can give many details at the atomic/molecular level. It is usually performed to simulate the pyrolysis of the individual principal biomass components, interactions within/between these materials, and catalytic pyrolysis with various catalysts. On the basis of the theoretical models in quantum chemistry modelling, geometric structures, transition states, intermediates, corresponding electron transfers, orbital interactions, energetics, and other important information involved in the pyrolysis process can be obtained. Benefiting from the advancement of theoretical methods and computer hardware, quantum chemistry modelling is playing increasingly important roles in the lignocellulosic biomass pyrolysis mechanism studies.

However, the majority of literature on biomass pyrolysis quantum chemical modelling has been found to have a low standard quantum chemical bias due to the absence of well-established and robust protocols in the field. The real danger lies in the scientific community of "non-theoretical chemists" persisting in the use of outdated functionals (such as B3LYP) simply due to their established history, rather than their demonstrated effectiveness. This issue has been highlighted by Grimme and his colleagues in their recent works [10, 11]. This low quality quantum chemical modelling can introduce a significant level of uncertainty in computed properties (in particular geometries and reaction barriers), especially when these data are incorporated into global kinetic schemes to reproduce pyrolysis experiments. Therefore, it is essential to develop new, more physically based protocols for accurate cost-effective characterization of lignocellulosic pyrolytic systems.

This paper presents a proposal to use β-D-xylopyranose (xylose) as a structural motif of hemicellulose. The thermal degradation potential energy surfaces (PESs) of xylose are investigated using density functional theory computations and composite schemes to uncover the energetics and thermodynamics of the associated chemical processes. Preliminary conformational analysis is also conducted to identify the global minimum conformer of the species under investigation. In addition, kinetic parameters are calculated using transition state theory (TST) for the elementary steps shown in Figure 1. Furthermore, for the first time, reaction barriers for the thermal degradation of xylose are calculated using a new family of composite schemes (junChS), as described in the Computational Methodology section. This establishes new reference data that could be useful for benchmarking purposes within the pyrolysis scientific community.

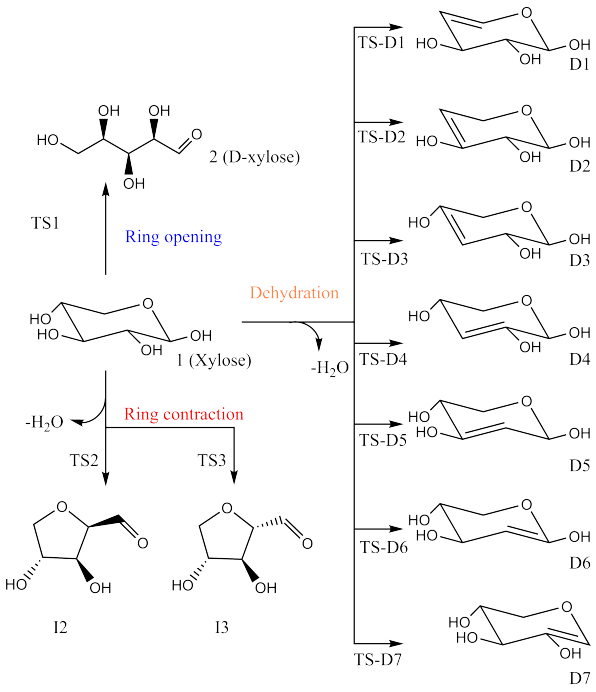

Figure 1: Initial steps of xylose thermal degradation: ring-opening, ring-contraction and dehydration.

Computational Methodology

The potential energy surfaces of the studied compounds were analyzed using composite model chemistry methods and density functional theory.

Composite model chemistry methods involve a stepwise approach to obtain accurate results in chemical calculations. These methods begin with initial calculations at a relatively simple and cost-effective level. The basis set is then extended to the complete basis set (CBS) limit, and higher levels of correlation energy, such as MP4 and perturbative triples excitations, are incorporated. Additionally, in some cases, empirical factors are added to correct for dissociation energies with respect to the atoms. By following this approach, composite model chemistry methods can improve the accuracy of chemical calculations without requiring highly expensive computational resources. Available methods comprise the CBS model chemistries reported by Petersson *et al.* [12, 13], the Gaussian-n (Gn) methods reported by Pople and co-workers [14], the Weizmann-n (Wn) theories reported by Martin and co-workers [15], the focal point method reported by Schuurman *et al.* [16], the "high accuracy extrapolated ab initio thermochemistry" (HEAT) method reported by Tajti *et al.* [17], and "cheap" schemes (ChS) methods by Barone and coworkers [18, 19]. In particular, in this paper, we used the CBS-QB3, G4 and junChS methods. The junChS total electronic energies are obtained by single-point computations at revDSD-PBEP86-D3(BJ)/jun-cc-pVTZ ge-

ometries [20]:

$$E_{\text{junChS}} = E(\text{CCSD(T)/jVTZ}) + \Delta E^{\text{CBS}}_{\text{MP2}} + \Delta E_{\text{CV}} \quad (1)$$

where the CBS term is

$$\Delta E^{\text{CBS}}_{\text{MP2}} = \frac{4^3 E(\text{MP2/jVQZ}) - 3^3 E(\text{MP2/jVTZ})}{4^3 - 3^3} - E(\text{MP2/jVTZ}) \quad (2)$$

and the core valence correction ΔE_{CV} is the MP2 energy difference between all electron (ae) and frozen core (fc) calculations employing the cc-pwCVTZ basis set. jVnZ stands for jun-cc-pVnZ basis set, where $n = T, Q$. Vibrational contribution (harmonic) is computed at the same level of theory of geometries.

On the grounds of its well-known robustness and widespread use [10, 11, 21], geometry optimizations and zero-point corrected electronic energies of reactants, transition states, intermediates, and products along the reaction pathways were obtained by the M06-2X [22] global hybrid density functional in conjunction with the 6-311++G(d,p) basis set. The stationary points on the reaction pathways were characterized as minima (reactants, intermediates, and products) and saddle points (transition states) based on vibrational frequency calculations. The transition states obtained were further confirmed using intrinsic reaction coordinate (IRC) scans at the same levels of theory.

Thermochemical quantities (Gibbs free energies, G) have been computed using the Shermo code [23], employing the standard standard rigid-rotor harmonic-oscillator (RRHO) approximation. The code treats automatically low frequencies employing Grimme's entropy interpolation between harmonic and free-rotor approximations.

Given the high flexibility of the molecules under investigation, conformational analysis for minima and transition states is performed with CREST program [24] in order to provide starting guesses for the potential energy surfaces calculations. The code couples state-of-art semiempirical quantum chemical methods (GFNn-xTB) [25] with metadynamics simulations [26]. All geometry optimizations as well as energy, thermodynamic functions and frequency calculations have been performed using the Gaussian code [27]. Rate coefficients are determined by the conventional transition state theory (TST) within the rigid-rotor harmonic-oscillator (RRHO) approximation, and they can be expressed by

$$k(T) = \kappa(T) \frac{m^{\ddagger} \sigma_{ext}}{m \sigma^{\ddagger}_{ext}} \frac{k_B T}{h} \frac{Z^{\ddagger}}{Z} \exp\left(-\frac{E_0}{k_B T}\right). \quad (3)$$

Here $\kappa(T)$ is the transmission coefficient, which accounts for tunneling as well as nonclassical reflection effects using the one-dimensional asymmetric Eckart model. $m^{\ddagger}$ and m denote the number of enantiomers for the transition state and reactants, respectively, while σ_{ext} and σ refer to the symmetry numbers for external rotation of these entities. The partition functions for the transition state and reactants are denoted by $Z^{\ddagger}$ and Z, respectively. Furthermore, the constants h, T, and k_B represent Planck's constant, temperature, and Boltzmann's constant, respectively. The term E_0 represents the barrier height, including the zero-point energy. To model their temperature dependence, the rate constants at different temperatures have been fitted to Arrhenius equation

$$k(T) = A \exp\left(-\frac{E_a}{RT}\right). \quad (4)$$

The TST calculations have been performed using MESS code by Georgievskii *et al.* [28].

Results

Table 1: Xylose thermal degradation relative standard enthalpies at 0 K ($\Delta H^{\circ}_{0\,\text{K}}$) (i.e., zero-point corrected electronic energies). In particular, initial step of the three main pathways are reported, i.e., ring opening, ring contraction, and dehydration ones. Values in kJ mol^{-1}.

		M06-2X	CBS-QB3	G4	junChS
Ring opening	Xylose	0.00	0.00	0.00	0.00
	TS1	184.77	184.88	181.79	183.09
	2	16.92	18.90	20.10	17.34
Ring contraction	TS2	304.06	-	298.81	292.82
	TS3	292.98	-	272.26	271.16
	I2 + H_2O	55.02	41.51	40.96	39.17
	I3 + H_2O	56.87	43.35	41.58	41.64
Dehydration	TS-D1	279.20	279.08	276.48	276.25
	TS-D2	293.19	290.90	289.66	288.34
	TS-D3	295.99	291.73	288.81	288.06
	TS-D4	291.58	291.50	288.95	287.17
	TS-D5	305.44	305.51	303.44	300.54
	TS-D6	345.09	341.12	340.54	337.12
	TS-D7	285.24	285.53	283.84	278.68
	D1 + H_2O	31.97	24.26	21.86	18.86
	D2 + H_2O	35.45	28.74	26.96	21.91
	D3 + H_2O	32.93	25.28	22.86	19.43
	D4 + H_2O	38.84	29.88	27.77	23.74
	D5 + H_2O	36.70	27.17	25.33	21.18
	D6 + H_2O	23.18	16.67	14.83	10.20
	D7 + H_2O	63.45	55.75	53.76	49.73
	MAX	21.82	6.85	5.98	
	MUE	9.68	4.17	2.71	
	RMSD	11.33	4.65	3.23	

Investigation of xylose pyrolysis initial reaction steps has been performed and results are reported in this Section. Xylose can undergo 3 different initial reactions, ring opening, ring contraction and dehydration reactions, as detailed in Figure 1. Zero-point corrected electronic energies computed at different levels of theory are gathered in Table 1. In particular the performances of M06-2X/6-311++G(d,p) (hereafter M06-2X), CBS-QB3 and G4 are compared to those of junChS. Among CBS-QB3 and G4, the latter provides smaller errors, as already reported in literature [29], showing a Root-mean-square deviation (RMSD) of 3.23 kJ mol^{-1} with respect to 4.65 kJ mol^{-1}. M06-2X shows overall satisfactory performances, with a RMSD of 11.33 kJ mol^{-1}. At the CBS-QB3 level of theory, it

was not possible to locate the transition states TS2 and TS3 for the ring contraction reactions.

Looking at Table 2, it is notable that the ring opening product (2) is not thermodynamically favourable for the investigated reaction across the entire temperature range (300-1000 K), while both ring contraction and dehydration mechanisms are favourable. Interestingly, the dehydration product, D7 + H_2O, is unfavourable at 300 and 400 K, but becomes favourable at 500 K.

Table 2: Xylose thermal degradation relative free energies (ΔG) at various temperatures. In particular, initial step of the three main pathways are reported, i.e., ring opening, ring contraction, and dehydration ones. Computed at M06-2X/6-311++G(d,p) level of theory. Values in kJ mol^{-1}.

	T /K	300	400	500	600	700	800	900	1000
Ring opening	1 Xylose	0.00	0.00	0.00	0.00	0.00	0.00	0.00	0.00
	TS1	186.46	187.79	189.32	190.99	192.77	194.63	196.57	198.56
	2	15.28	14.68	14.11	13.55	13.03	12.54	12.09	11.67
Ring contraction	TS2	302.70	302.31	301.95	301.65	301.42	301.27	301.19	301.19
	TS3	291.69	290.97	290.20	289.43	288.70	288.01	287.37	286.79
	I2 + H_2O	10.94	-5.84	-22.60	-39.26	-55.78	-72.14	-88.35	-104.40
	I3 + H_2O	12.71	-4.16	-21.02	-37.80	-54.44	-70.93	-87.27	-103.45
Dehydration	TS-D1	280.58	281.19	281.70	282.13	282.50	282.82	283.12	283.40
	TS-D2	294.16	294.53	294.80	294.99	295.12	295.21	295.28	295.33
	TS-D3	296.30	296.26	296.12	295.90	295.61	295.29	294.96	294.61
	TS-D4	291.25	291.17	291.02	290.82	290.60	290.38	290.16	289.96
	TS-D5	304.41	304.05	303.65	303.23	302.80	302.40	302.02	301.68
	TS-D6	343.38	342.56	341.66	340.70	339.71	338.73	337.77	336.84
	TS-D7	282.70	281.44	280.11	278.75	277.41	276.09	274.82	273.59
	D1 + H_2O	-9.37	-25.24	-41.26	-57.30	-73.30	-89.24	-105.07	-120.80
	D2 + H_2O	-6.89	-23.25	-39.74	-56.24	-72.68	-89.03	-105.26	-121.37
	D3 + H_2O	-9.42	-25.70	-42.11	-58.53	-74.89	-91.16	-107.31	-123.35
	D4 + H_2O	-3.67	-19.96	-36.36	-52.76	-69.09	-85.32	-101.43	-117.41
	D5 + H_2O	-5.84	-22.10	-38.46	-54.80	-71.07	-87.23	-103.26	-119.16
	D6 + H_2O	-20.34	-37.28	-54.37	-71.48	-88.54	-105.50	-122.35	-139.09
	D7 + H_2O	20.90	4.36	-12.34	-29.07	-45.74	-62.33	-78.81	-95.17

The rate coefficients were calculated within the temperature range of 300 to 1000 K using reaction barriers computed at the junChS level of theory (refer to Table 1). The temperature dependence rate constants plot is presented in Figure 2. As previously noted in the literature [30, 31], ring opening is the fastest reaction channel throughout the entire temperature range. The other reaction channels are slower by 1-2 orders of magnitude, which means that, kinetically, ring opening is always favourable. The Arrhenius plots indicate that the investigated reactions follow the expected Arrhenius behavior within the temperature range studied. However, for dehydration reactions involving TS-D4, TS-D5, and TS-D6, there are slight deviations from the trend at lower temperatures.

Table 3: Fitted Arrhenius parameters.

	A /s^{-1}	E_a /kJ mol^{-1}
Ring opening	5.07×10^{12}	181.34
Ring contraction (TS2)	5.21×10^{14}	300.86
Ring contraction (TS3)	5.51×10^{13}	277.30
Dehydration (TS-D1)	1.40×10^{13}	279.38
Dehydration (TS-D2)	1.71×10^{13}	292.14
Dehydration (TS-D3)	3.42×10^{13}	293.13
Dehydration (TS-D4)	7.48×10^{13}	289.43
Dehydration (TS-D5)	1.91×10^{14}	303.56
Dehydration (TS-D6)	5.43×10^{14}	340.82
Dehydration (TS-D7)	6.18×10^{14}	287.97

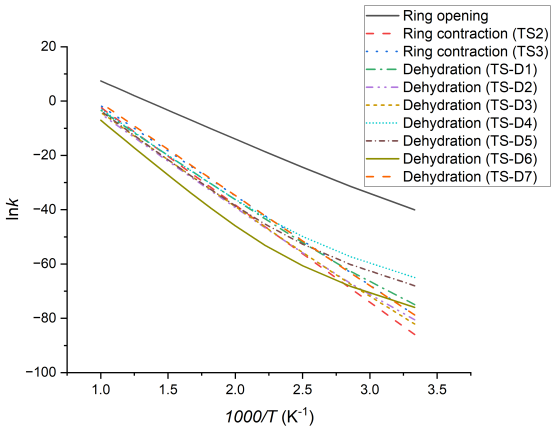

Figure 2: Arrhenius plots illustrate the temperature-dependent rate coefficients in the initial stages of xylose pyrolysis.

Conclusions

In this study, β-D-xylopyranose has been proposed as a structural motif to model hemicellulose. Initial reaction steps, including ring opening, ring contraction, and dehydration, were investigated using quantum chemical calculations. Energetic results align well with previous literature findings and provide new reference data at the junChS level of theory. These data can serve as a valuable benchmark for future studies. Additionally, TST results will aid in the development of a global kinetic scheme for xylose pyrolysis in future research.

Acknowledgements

The research was supported by fundings from the Ryanair Sustainable Aviation Research Center at Trinity College Dublin, the European Union through the European Research Council, Mod-L-T, action number 101002649, and the Science Foundation Ireland (SFI) under grant number 12/RC/2278_2. The authors wish to acknowledge the Irish Centre for High-End Computing (ICHEC) for the provision of computational facilities and support.

References

[1] European Commission and Directorate-General for Communication, *European green deal: delivering on our targets* (Publications Office of the European Union, 2021).

[2] S. Wang, G. Dai, H. Yang, and Z. Luo, Lignocellulosic biomass pyrolysis mechanism: A state-of-the-art review, *Prog. Energy Combust. Sci.* **62**, 33 (2017).

[3] E. Ranzi, M. Corbetta, F. Manenti, and S. Pierucci, Kinetic modeling of the thermal degradation and combustion of biomass, *Chem. Eng. Sci.* **110**, 2 (2014).

[4] P. E. A. Debiagi, C. Pecchi, G. Gentile, A. Frassoldati, A. Cuoci, T. Faravelli, and E. Ranzi, Extractives extend the applicability of multistep kinetic scheme of biomass pyrolysis, *Energy Fuels*

29, 6544 (2015).

[5] P. E. A. Debiagi, G. Gentile, M. Pelucchi, A. Frassoldati, A. Cuoci, T. Faravelli, and E. Ranzi, Detailed kinetic mechanism of gas-phase reactions of volatiles released from biomass pyrolysis, *Biomass Bioenergy* **93**, 60 (2016).

[6] E. Ranzi, P. E. A. Debiagi, and A. Frassoldati, Mathematical modeling of fast biomass pyrolysis and bio-oil formation. Note I: Kinetic mechanism of biomass pyrolysis, *ACS Sustainable Chem. Eng.* **5**, 2867 (2017).

[7] K. Dussan, S. Dooley, and R. Monaghan, Integrating compositional features in model compounds for a kinetic mechanism of hemicellulose pyrolysis, *Chem. Eng. J.* **328**, 943 (2017).

[8] K. Dussan, S. Dooley, and R. Monaghan, A model of the chemical composition and pyrolysis kinetics of lignin, *Proc. Combust. Inst.* **37**, 2697 (2019).

[9] S. Dooley, S. H. Won, M. Chaos, J. Heyne, Y. Ju, F. L. Dryer, K. Kumar, C.-J. Sung, H. Wang, M. A. Oehlschlaeger, et al., A jet fuel surrogate formulated by real fuel properties, *Combust. Flame* **157**, 2333 (2010).

[10] M. Bursch, J.-M. Mewes, A. Hansen, and S. Grimme, Best-practice DFT protocols for basic molecular computational chemistry, *Angewandte Chemie International Edition* **61**, e202205735 (2022).

[11] L. Goerigk, A. Hansen, C. Bauer, S. Ehrlich, A. Najibi, and S. Grimme, A look at the density functional theory zoo with the advanced GMTKN55 database for general main group thermochemistry, kinetics and noncovalent interactions, *Phys. Chem. Chem. Phys.* **19**, 32184 (2017).

[12] J. A. Montgomery, M. J. Frisch, J. W. Ochterski, and G. A. Petersson, A complete basis set model chemistry. VI. Use of density functional geometries and frequencies, *J. Chem. Phys.* **110**, 2822 (1999).

[13] J. A. Montgomery, M. J. Frisch, J. W. Ochterski, and G. A. Petersson, A complete basis set model chemistry. VII. Use of the minimum population localization method, *J. Chem. Phys.* **112**, 6532 (2000).

[14] L. A. Curtiss, P. C. Redfern, and K. Raghavachari, Gaussian-4 theory, *J. Chem. Phys.* **126**, 084108 (2007).

[15] A. Karton and J. M. L. Martin, Explicitly correlated Wn theory: W1-F12 and W2-F12, *J. Chem. Phys.* **136**, 124114 (2012).

[16] M. S. Schuurman, S. R. Muir, W. D. Allen, and H. F. Schaefer, Toward subchemical accuracy in computational thermochemistry: Focal point analysis of the heat of formation of NCO and [H,N,C,O] isomers, *J. Chem. Phys.* **120**, 11586 (2004).

[17] A. Tajti, P. G. Szalay, A. G. Császár, M. Kállay, J. Gauss, E. F. Valeev, B. A. Flowers, J. Vázquez, and J. F. Stanton, HEAT: High accuracy extrapolated ab initio thermochemistry, *J. Chem. Phys.* **121**, 11599 (2004).

[18] S. Alessandrini, V. Barone, and C. Puzzarini, Extension of the "cheap" composite approach to noncovalent interactions: The jun-ChS scheme, *J. Chem. Theory Comput.* **16**, 988 (2020).

[19] J. Lupi, S. Alessandrini, C. Puzzarini, and V. Barone, junChS and junChS-F12 models: Parameter-free efficient yet accurate composite schemes for energies and structures of noncovalent complexes, *J. Chem. Theory Comput.* **17**, 6974 (2021).

[20] G. Santra, N. Sylvetsky, and J. M. L. Martin, Minimally empirical double-hybrid functionals trained against the GMTKN55 database: revDSD-PBEP86-D4, revDOD-PBE-D4, and DOD-SCAN-D4, *J. Phys. Chem. A* **123**, 5129 (2019).

[21] B. Hu, B. Zhang, W. Xie, X. Jiang, J. Liu, and Q. Lu, Recent progress in quantum chemistry modeling on the pyrolysis mechanisms of lignocellulosic biomass, *Energy Fuels* **34**, 10384 (2020).

[22] Y. Zhao and D. G. Truhlar, The M06 suite of density functionals for main group thermochemistry, thermochemical kinetics, noncovalent interactions, excited states, and transition elements: two new functionals and systematic testing of four M06-class functionals and 12 other functionals, *Theor. Chem. Acc.* **120**, 215 (2008).

[23] T. Lu and Q. Chen, Shermo: A general code for calculating molecular thermochemistry properties, *Comput. Theor. Chem.* **1200**, 113249 (2021).

[24] P. Pracht, F. Bohle, and S. Grimme, Automated exploration of the low-energy chemical space with fast quantum chemical methods, *Phys. Chem. Chem. Phys.* **22**, 7169 (2020).

[25] C. Bannwarth, E. Caldeweyher, S. Ehlert, A. Hansen, P. Pracht, J. Seibert, S. Spicher, and S. Grimme, Extended tight-binding quantum chemistry methods, *Wiley Interdiscip. Rev. Comput. Mol. Sci.* **11**, e1493 (2021).

[26] S. Grimme, Exploration of chemical compound, conformer, and reaction space with metadynamics simulations based on tight-binding quantum chemical calculations, *J. Chem. Theory Comput.* **15**, 2847 (2019).

[27] M. J. Frisch, G. W. Trucks, H. B. Schlegel, G. E. Scuseria, M. A. Robb, J. R. Cheeseman, G. Scalmani, V. Barone, G. A. Petersson, H. Nakatsuji, et al., Gaussian 16 Revision C.01 (2016), Gaussian Inc. Wallingford CT.

[28] Y. Georgievskii, J. A. Miller, M. P. Burke, and S. J. Klippenstein, Reformulation and solution of the master equation for multiple-well chemical reac-

tions, *J. Phys. Chem. A* **117**, 12146 (2013).

[29] J. M. Simmie and K. P. Somers, Benchmarking compound methods (CBS-QB3, CBS-APNO, G3, G4, W1BD) against the active thermochemical tables: A litmus test for cost-effective molecular formation enthalpies, *J. Phys. Chem. A* **119**, 7235 (2015).

[30] H. Bin, L. Qiang, X. Z. Zhen, T. W. Yu, L. Kai, Q. D. Chang, and P. Y. Yong, Mechanism insight into the fast pyrolysis of xylose, xylobiose and xylan by combined theoretical and experimental approaches, *Combust. Flame* **206**, 177 (2019).

[31] J. Huang, C. He, L. Wu, and H. Tong, Thermal degradation reaction mechanism of xylose: A DFT study, *Chem. Phys. Lett.* **658**, 114 (2016).